J. Mat. NanoSci. 2014, 1(1), 31-38 Review

Journal of
Materials NanoScience

Nanomagnetic Thinfilms for Advanced Inductors and EMI Shields in Smart Systems

P. Markondeya Raj, Dibyajat Mishra, Srikrishna Sitaraman and Rao Tummala

3D Systems Packaging Research Center, Georgia Institute of Technology, Atlanta, GA,USA

Received Date: 05-July-2014

ABSTRACT

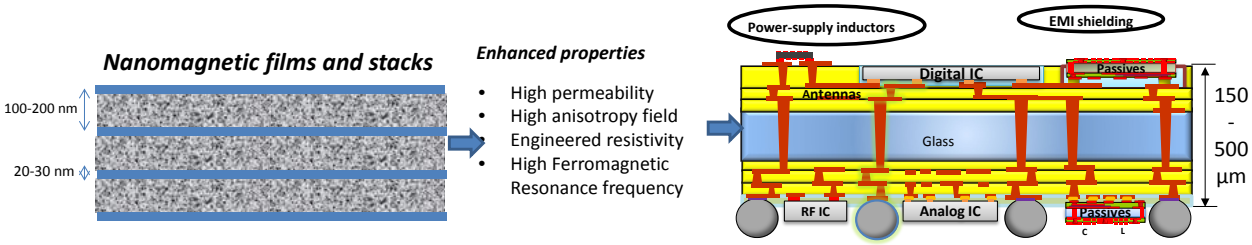

Nanomagnetics provide unique opportunities to address the fundamental limitations of traditional electronic materials for miniaturization of RF and power components, while simultaneously enhancing their performance. This paper demonstrates nanomagnetic films and processes for power inductors and EMI shield applications. A DC-RF co-sputtering process was developed to synthesize cobalt-based nanogranular films with superior properties compared to microscale magnetic materials. The benefits of this material for miniaturized power inductors are demonstrated with analytical models. The second part of the paper demonstrates miniaturization of electromagnetic interference (EMI) shields with nanomagnetic film-stacks.

Keywords: Nanomagnetics, Inductors, EMI Shields, Thin Films, Smart Systems

INTRODUCTION

The emergence of smart phones is driving a new need in electronics system technologies, requiring a new focus in system scaling for system components such as package substrates, passive components, thermal structures, power sources and interconnections. Current system components are at milliscale structural dimensions with microscale materials, resulting in a 10^3-10^6 scaling gap with the transistors. In addition, with existing materials, component miniaturizationdegrades electrical and mechanical performance metrics such as thermomechanical stability, quality factor, leakage currents, tolerance or precision, thermal and frequency-stability. Nanomaterials and processescan miniaturize these milliscale system components to microscale structures in the near future and eventually to nanoscale, while simultaneously enhancing the performance. These nanocomponents can then be assembled close to the active devices such as digital and RF (radio frequency) ICs (integrated circuits), either as thin films or 3D integrated passive devices (3D IPDs) resulting in ultra-miniaturized and ultra-thin systems with unique 3D integration of passives with active components (3D IPAC). Majority of these system components comprise of passive components which form the key focus of this paper.

The primary examples of passive components are inductors, capacitors, resistors, circulators, isolators, electromagnetic interference (EMI) shield structures, antennas etc. that support the active components to perform various functions in power and RF modules such as voltage conversion, noise suppression, amplification, filtering etc. The focus of this article is to describe

Corresponding Author: Dr. P. Markondeya Raj
Tel: (001) 404 558 2615
Email: raj@ece.gatech.edu

Cite as: *J. Mat. NanoSci., 2014, 1(1), 31-38.*

the role of nanomagnetic materials, structures and processes in miniaturizing today's bulky passive components into thinfilms or thin devices with enhanced volumetric density, quality factor and frequency stability, as illustrated in Figure. 1. The figure illustrates six classes of applications for nanomagnetic materials in system module with 3D integration of passives and actives for a future smart system.

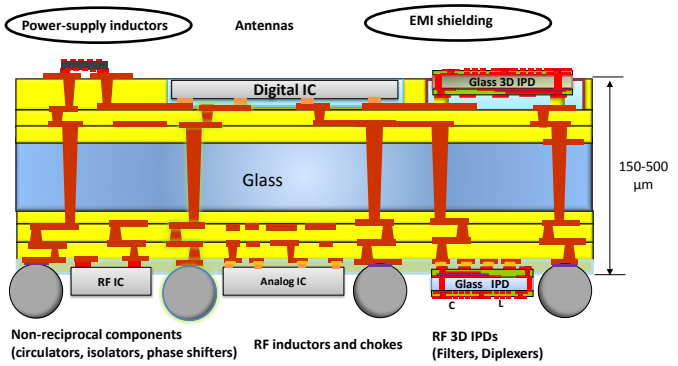

Figure 1. Applications of nanomagnetics in highly-integrated modules and sub-systems. The highlighted items are the key focus of this paper.

Subsequent sections describe nanomagnetic films for advancing two system components. The first part of the paper describes high-density inductors for power applications using sputtered nanomagnetic films. The role of such nanomagnetic films in creating compact EMI shield structures between embedded RF and mixed-signal components is demonstrated in the second part of the paper. A brief overview of the state-of-the-art nanomagnetics research is also provided.

MICRO VS NANOMAGNETICS

The key magnetic properties for both power and RF passive components are permeability, saturation magnetization, anisotropy field which determines the current-handling, loss tangent and frequency-stability. The limitations of micromagnetics in achieving this combination of properties are briefly discussed in this section, followed by a summary of recent R&D advances in nanomagnetics to overcome these limitations.

Micromagnetics: Ferrites, ferrite composites or metal composites are the most common magnetic materials used for thin-film passive power components today. However, they face fundamental limitations in achieving the required properties and processability for future applications. Ferrites have inherent process integration challenges and low saturation magnetization that limit their volumetric density, and in addition, show poor frequency stability. Traditional metal-based magnetic composites at submicro or microscale also do not show adequate frequency-stability and low loss. The eddy current losses are directly proportional to the particle size and are, therefore, higher for microscale particles.[1] Larger particles also have multiple domains thatgenerate additional losses from the domain wall resonance.[1-3] Several studies have been reported on magnetic metal-polymer composites, particularly focusing on the iron-polymer and NiFe-polymer systems.[4,5] With large microsized particles, permeabilities of above 100 are reported. These particles show lower coercivity and higher intrinsic permeability. However, the magnetic losses become significant even at 1 MHz. These limitations are overcome by nanomagnetics and discussed next.

Particulate nanocomposites: Higher permeability and improved frequency-stability can be achieved in magnetic nanocomposites by reducing the particle size and the separation between the neighboring metal particles down to the nanoscale. Because of the nanosized metal particles, the eddy currents produced within the particle are also negligibly small, leading to much lower loss for nanocomposites, compared to that of conventional microsized ferrites and powder materials. As the particle size is reduced down to the nanoscale, the particle size and exchange length converge, allowing for single domain states to stabilize, resulting in the elimination of domain-wall losses. The exchange coupling interaction extends out to the neighboring grains within a characteristic distance, l_{ex} which is ~20 nm for Co.[6,7] The exchange interaction in nanocomposites also leads to the cancellation of magnetic anisotropy of individual particles and the demagnetizing effect, leading to higher permeability and lower coercivity.[8,9] The effective anisotropy for the magnetic behavior is averaged over several grains and, thus, reduced in magnitude. Co- or Fe-based nanocomposites show much higher permeability at microwave frequencies than those obtained from the bulk Co or Fe metal or their microscale composites.[10-13] The cancellation of effective magnetocrystalline anisotropy by exchange coupling also allows easy magnetic orientation with an external applied field in order to control the magnetic properties in the target directions.

Several metal-metal oxide nanocomposites were shown to have high permeability and low coercivity in the hard-axis direction, along with high resistivity.[12-14] These comprise of metals such as Co, Ni, Fe or their alloys in an oxide matrix of metals with high oxide affinity such as Si, Hf, Zr. For example, Fe-Co-Hf-O films showed low coercivity of less than 1 Oe and high field anisotropy in the hard axis.[15] Such nanomagnetic structures with high permeability and low loss were mostly obtained through sputtering and cannot yield thick magnetic films. Nanoparticle composites in polymer matrices that are synthesized via chemical synthesis routes can accomplish thick films. However, they do not show such high permeability as sputtered films because of the absence of exchange coupling. Their isotropic nature also results in FMR-broadening and higher losses.[16,17]

Nanowire structures: Anisotropic one-dimensional nanostructures based on nickel or cobalt nanowires or filaments show enhanced FMR and suppressed FMR-broadening to overcome the limitations of isotropic nanocomposites.[18] Nanowire composites with crystallographically oriented cobalt of high magnetocrystalline field anisotropy showed a permeability of 3.5 and loss of 0.045 till 4.5 GHz, in a recent study.[19]

Nanolaminate structures: Higher frequency stability and lower losses can also be achieved with two-dimensional nanostructures. Two types of such nanocomposites are being explored: 1.) Nanoflake composites and 2.) Layered nanomagnetic structures. Studies on NiFe alloy flake-polymer nanocomposites showed permeabilities of 5-10 with losses of above 0.1 at 1 GHz.[20] In another study by Yang et al., oriented flake-shaped Fe alloy particles mixed in a paraffin matrix showed a permeability of 8 at 100 MHz and 3.9 upto 2 GHz.[21,22] Oriented

ferrite films with hard-axis perpendicular to the film plane are also shown to enhance frequency stability.[22]

Nanolaminate structures that are designed to have strong exchange coupling at the ferromagnetic-antiferromagnetic interfaces are expected to have high FMR and permeability. The thickness of the ferromagnetic layer is used to control the FMR at the expense of the permeability, in a study by Sonehara et al.[23] Chai et al.[24] have shown that nanolaminates with (Co96-Zr4/Cu)n multilayers have higher frequency stability than predicted by Acher's limit, by engineering the interface anisotropy. Utilization of nanolaminates to optimize frequency stability and permeability is a promising avenue for enabling miniaturized magnetic devices in multi GHz range.

This paper applies advances in nanomagnetic films to two components in smart systems – power inductors and EMI shields.

NANOMAGNETIC INDUCTORS

For power and RF inductors, nanomagnetics enhance the inductance density while retaining GHz stability, low losses and high current-handling. The key magnetic structural attributes that leads to these advantages are low eddy current losses from high resistivity, low coercivity, and enhanced permeability. In addition, high anisotropy field is critical for both power and RF applications. In power applications, they are critical for high power-handling and low hysteresis losses in the hard-axis. For both power and RF applications, magnetic anisotropy also leads to high ferromagnetic resonance frequency (FMR). The inductor size requirements can also be reduced by orders of magnitude by increasing the operation frequency.[25] However, at high frequencies, permeability decreases and the losses increase with microscale materials. This limitation can be addressed with nanomagnetic materials.

Inductor modeling:

The inductance (L) of a toroid inductor is given as:

$$L = \frac{\mu_o \mu_r A_c N^2}{l_c} = \frac{N^2}{R} \qquad (1)$$

where l_c is the length of the core, A_c is the cross-section area of the core, R is the reluctance, and N refers to the number of turns, μ_o and μ_r are the permeability of free space and relative permeability. A toroid design with target inductor attributes compiled in Table 1 is shown in Figure 2. The inductance density as a function of relative permeability is shown in figure 3a for the toroid design. A permeability of ~200 is required to achieve 300 nH/mm^2 with six turns, three on each side.

To achieve the target inductance, it is important to maximize the number of turns while enhancing the permeability. However, increasing the number of turns increases the coil resistance and, consequently, the joule-heating losses. The quality factor of the inductor, in its simplistic form considers only these resistance losses, and is defined as:

$$Q = \frac{\omega L}{Resistance} = \frac{\omega \mu_o \mu_r N A_c A_w}{2\rho W l_c} \qquad (2)$$

where A_w is the cross-sectional area of the conductor, ω is the radian frequency, $2W$ is the length of the coil per turn, and ρ is the resistivity of the conductor material. Increasing the number of turns compromises the Q by increasing the coil resistance.

The other magnetic loss mechanisms that need to be considered are: (a) hysteresis loss; (b) eddy current loss. The area inside the magnetic hysteresis loop corresponds to the energy loss per cycle. Hysteresis power loss is proportional to the loop area. Increased turns raise the magnetic field inside the core and consequently increase the core hysteresis losses. Therefore, a small coercivity (H_c) is required to minimize the loop area, and in turn, the hysteresis loss. The eddy current losses are inversely proportional to the electrical resistivity of the magnetic material. Therefore, cores with higher resistivity are desired.

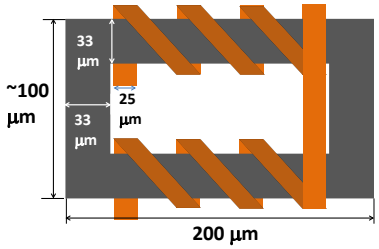

Figure 2. Exemplary inductor design to achieve the target properties compiled in Table 1.

Table 1. Inductor properties.

Property	Target
Inductance density	300 nH/mm^2
Frequency	100 MHz
Current-handling:	1 A/mm^2
Total loss	5%
DC losses:	<2.5% for 1A

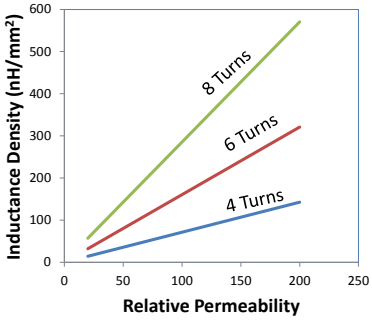

(a)

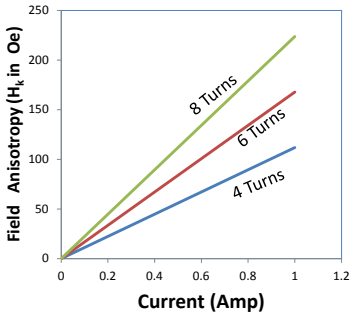

(b)

Figure 3. (a) Inductance density vs relative permeability for the design shown in figure 2. (b) Field anisotropy vs DC current in the inductor.

The DC current saturation (I_{sat}) is described by the equation:

$$I_{sat} = B_{sat}\frac{l_c}{N\mu_o\mu_r} = \frac{l_c H_k}{N} \quad (3)$$

where B_{sat} refers to the saturation flux density. Increase in the inductance density by increasing the number of turns saturates the inductor at lower DC currents, as seen from Equation (3). The inductor has to be designed such that the DC magnetization field is within the saturation field of the material, referred to as $B_{sat}/(\mu_o\mu_r)$ or H_k, the anisotropy field. By creating magnetic anisotropy, H_k can be dramatically increased in the hard axis for higher current-handling, however, at the expense of permeability. Figure 3b shows the plot of field anisotropy vs current thus obtained for different number of turns. Based on the plot, the required field anisotropy of the film, H_k, is estimated to be ~40 Oe for current-handling of 0.2 A (1 A/mm^2). The key target inductor properties, material properties and inductor design are shown in Table 2.

Table 2: Design to achieve target inductance.

Relative Permeability	~200
Anisotropy Field	40 Oe
Copper winding	Cross-section: 25μm ×25 μm; 6 Turns – 3 on each side
Inductor height:	60 μm;
Magnetic core	Thickness: 10 μm X-Y:100 ×200 μm

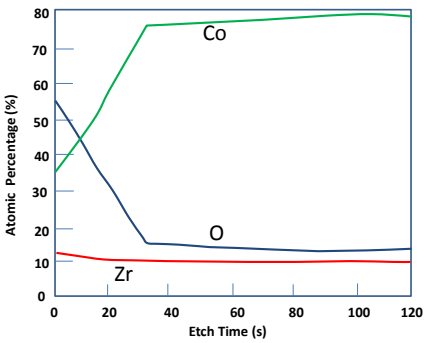

(a)

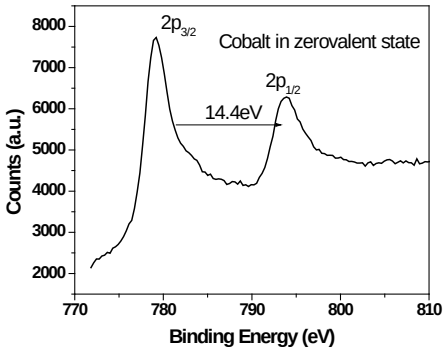

(b)

Figure 4. (a)XPS composition profile of the sputtered films; (b) cobalt 2p core level XPS spectrum.

MATERIALS AND CHARACTERIZATION

This section describes the materials and properties of DC-RF co-sputtered films to achieve the unique attributes for high-density inductors. With co-sputtered metal-metal oxide nanocomposites, electrical resistivity and anisotropy field can be adjusted by controlling the ratio between metal and metal oxide. Decreasing the metal/oxide ratio increases the electrical resistivity. On the other hand, to keep high enough saturation magnetization M_s, a high fraction of metal (Co, Fe, Ni) is desired. Favorable soft magnetic properties can only be obtained in a limited composition and thickness range. Co-Zr-O films are chosen because they possess high M_s, high anisotropy field (H_k) and soft magnetic properties over a much wider compositional range.

Co-Zr-O films were deposited in a DC-RF sputterer by co-sputtering of Co and Zr targets in an Ar+O_2 atmosphere on 4" Si wafers and glass substrates. The gases were introduced simultaneously into the sputtering chamber using two different mass flow controllers (MFCs) which help in controlling their ratios. Thus, by changing the power ratios of Co and Zr and the gas-flow ratios during sputtering, the composition of the sputtered film can be controlled. The thickness of the sputtered films, measured using a Tencor P15 profilometer, is 150-200 nm. The resistivity of the films is measured using a 4-point probe. The average resistivity of the sputtered films is 2.3x10^{-4} ohm-cm.

The composition of the films was measured using Thermo K-Alpha XPS using depth profiling which etches away the top few layers to obtain a representative film composition without the influence of the surface impurities. Figure 4a shows the composition profile of the sputtered films. The XPS spectra confirmed that cobalt is predominantly in zero-valence state (Figure 4b) with minor oxide shoulders, while zirconium is in the oxidized state.

The SEM cross-section of the film is shown in figure 5, further confirming the nanogranular nature of the film. TEM studies in the literature report that the cobalt forms a nanogranular structure of 1-2 nm[13,26] interspersed with the oxide. As described by the analysis of Herzer,[6] the nanogranular domains interact through exchange coupling when they are within the exchange length defined as:

$$L_{ex} = \sqrt{\left(\frac{A}{K}\right)} \quad (4)$$

where A is the exchange constant and K is the anisotropy energy density. The effective anisotropy is reduced by a factor of $\sqrt{N}$, where N is defined as the number of exchange-coupled grains within the exchange volume:

$$N = \left(\frac{L_{ex}}{D}\right)^3 \quad (5)$$

The smaller grain size suppresses the effective magnetocrystalline anisotropy.

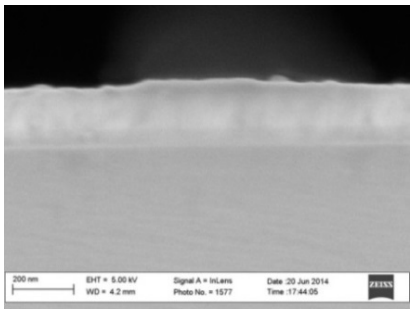

Figure 5. Nanomagnetic Co-Zr-O films from co-sputtering. The film thickness is 150-180 nm.

Fabricating a monolithic thick film increases the eddy current losses due to its relatively high conductivity. Thicker films also degrade the softness by forming unfavorable columnar structures causing stripe-domains or perpendicular anisotropy.[27] Hence, thicker films are fabricated as multilayered stacks of nanomagnetic films separated by oxide inter-layers to minimize eddy current losses and also preserve the soft nanomagnetic structure.[26] The target film thickness is thus achieved for the required inductance density and current-handling without sacrificing the inductor performance.

Nanomagnetic Characterization: When a unidirectional magnetic field is applied during deposition, a corresponding magnetic anisotropy with low coercivity in the hard-axis direction is created in the film. The anisotropic magnetic properties of the films were measured using vibration sample magnetometry (Lakeshore 736 Model). The tool also identifies the easy and hard axis directions of the film and measures the properties along them. The deposited multilayered films have high permeability, high saturation magnetization, and in-plane magnetic anisotropy, as shown by the B-H loop in Figure 6. Good in-plane anisotropy with high field anisotropy of 50 Oe and low coercivityof 3.7 Oe were measured from the loop. The high resistivity and low coercivity are expected to result in low losses.The properties of the deposited films, consistent with the inductor targets and design in Tables 1 and 2, are compiled in Table 3.

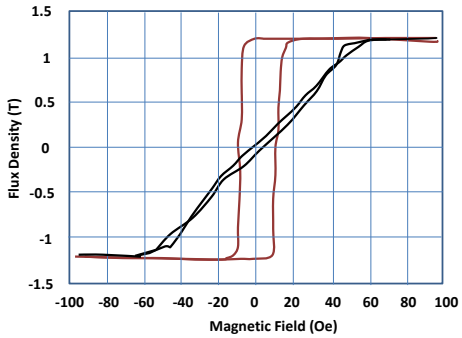

Figure 6. B-H loop of deposited Co-Zr-O films showing low coercivity in the hard-axis and high permeability.

Table 3: Properties of Co-Zr-O films.

Material	Co-Zr-O
Relative Permeability	~200
Thickness	150-200 nm
Coercivity	3.7 Oe
Anisotropy field	40-50 Oe
Saturation magnetization	1.2 Tesla
Resistivity	230 micro ohm cm

NANOMAGNETIC EMI SHIELDING STRUCTURES

A miniaturized multifunctional system houses several active and passive components in close proximity. All of them radiate electromagnetic (EM) fields of different strengths and frequencies. The region around an EM source is divided into near-field (distance < $\lambda/2\pi$) and far-field (distance > $\lambda/2\pi$). The usual separation distance between components is around 2-6mm. This means the components lie in the near-field region of each other even up to 8GHz. Additionally, the components also lie in the far-field region of external EM interference arising outside the package. Therefore, all components require electromagnetic interference (EMI) shields to prevent external interference from entering into the components, and also to suppress any radiation arising from the component. To this end, nanomagnetics provide the ability to design and create unique EMI isolation thinfilms instead of the metallic cans made from today's microscale materials[28] or spray-coated paints.[29] Magnetic thin films can also effectively create isolation in both vertical and horizontal directions, providing unique opportunities for 3D integrated modules and systems.

Fundamentally, EM shielding is effected through the following mechanisms[30]:

1.) Reflection loss is an interfacial phenomenon arising because of the difference in the impedance between the medium around the shield and the shield material. The reflection loss is different for far-field and near-field regions. In the near-field region, it is higher for electric than formagnetic fields. The expression for near-field magnetic field reflection loss is given by:

$$R_m = 20 \log \left(\frac{Z_w}{4|Z_s|}\right) \text{ dB} \quad (6)$$

Z_s is the impedance of the shield metal (unit ohms) given by:

$$Z_s = \sqrt{\frac{\omega \mu_m}{\sigma}} \quad (7a)$$

where ω is the angular frequency given by '$2\pi f$'; μ_m is the permeability of the shield metal, and σ is the conductivity of the shield metal specified in mhos/meter. Z_w is the near-field wave impedance (unit ohms) of magnetic fields given by

$$Z_w = 2\pi f \mu_w r \quad (7b)$$

where f is the frequency of radiation, μ_w is the permeability of the material surrounding the shield, r is the distance from source to shield.

2.) Absorption loss, observed in the bulk of the material, occurs because of the waves getting attenuated inside the metal. Absorption loss is defined by:

$$A = 15.6 t \sqrt{f \mu \sigma} \text{ dB} \quad (8)$$

where t is the thickness and μ is the permeability of the shield metal, and σ is the conductivity of the shield metal specified in mhos/meter.

Unlike electric fields, the low wave-impedance of magnetic fields in the near-field region makes it difficult to shield them through reflection loss. Usually, a shield with high absorption loss is used – which can be achieved through one of the following properties: large shield thickness, high conductivity, or high permeability. However, in ultra-miniaturized systems where the metal thickness cannot be high enough, absorption loss is not a major contributor to the shield effectiveness. Hence a shield that

can provide good reflection loss is preferred. This paper explores nanomagnetic films for shielding. However, there are two points of consideration with thin magnetic shields:

1.) The shield effectiveness decreases because of multiple-reflections inside thinner shields with low absorption loss. This is defined as[31]:

$$B = 20 \log_{10}(1 - qe^{-2t/\delta}) \text{ dB} \quad (9a)$$

where t is the thickness, δ is the skin depth of the shield metal in meters and q is the ratio between impedance of the shield (Z_m) and wave impedance (Z_w), defined by

$$q = \frac{(Z_w - Z_m)^2}{(Z_w + Z_m)^2} \quad (9b)$$

2.) With magnetic materials, the frequency stability of the permeability determines the applicability of the material, and is dictated by the FMR (ferromagnetic resonance) frequency. Because of the above-described phenomena of absorption or reflection, for the material to act as a shield, the FMR has to be higher than the frequency of interest. The FMR is related to the effective field anisotropy, and is written as:

$$F_{FMR} = \frac{\gamma}{2\pi} H_{Eff} \quad (10)$$

For a thin film with magnetic anisotropy, this resonance frequency is given by:

$$\frac{\omega_{FMR}}{\gamma} = \sqrt{(4\pi M_s + H)H} \quad (11)$$

H is the applied field or the anisotropy field H_k(in Oe), $4\pi M_s$ is the saturation magnetization (in Gauss) and γ is the gyromagnetic ratio (2.31 x 10^8 m/kAs). The equation can be further simplified as

$$FMR\ (MHz) \sim 2.8\sqrt{(Sat.Magnetization)H_k} \quad (12)$$

The structure, composition and magnetic anisotropycan be designed to tune the FMR, resistivity and permeability in order to create EMI isolation in the target frequency band. For materials with uniaxial anisotropy, the inherent frequency-stability and magnetic loss are governed by the saturation magnetization (M_s) and field anisotropy (H_k). Therefore, materials with high M_s and H_k are critical for high-frequency (GHz range) EMI shielding with reflection and absorption losses. However, it is important to note that the FMR itself can cause shielding because of the resonance-assisted microwave absorption.

CoZr and NiFe are considered for their EMI shielding performance. The properties measured by Gardner et al.,[32] Ha et al.,[26] Ohnuma et al. ,[13] and Yu et al.[33] are considered as guidelines for the properties used in the simulation. The properties of these systems are compiled in Table 4. The FMR values in the last column are estimated from Equation (12).

Table 4: Nanomagnetic systems for EMI shielding.

Material	H_k(Oe)	Perm.	Resistivity	FMRG Hz
M_s (kG)			μ ohm cm	
CoZr (16)	80	200	100	3.25
NiFe (9)	22.5	400	50	1.2

Analytical calculations based on Equations 6-9, (without FMR effects) were performed to estimate the shield effectiveness of the nanomagnetic material for a distance between source and shield of 5mm – the typical separation distance in a miniaturized system. The simulation considers0.1-3GHz since most RF and digital modules operate in these frequencies. Moreover, this analysis is to illustrate the impact of material properties. The effect of shield geometry and apertures on the shield effectiveness isignored.

The nanomagnetic films are assumed as 200nm thick layers. For multi-layer stacks, a 20nm thick layer of alumina is used between two successive nanomagnetic layers. For Co-Zr and NiFe systems, the shielding effectiveness of single-layer and multi-layer (10 layers) stack are studied and compared till their FMR frequencies – after which the FMR absorption comes into effect to provide the necessary shielding.

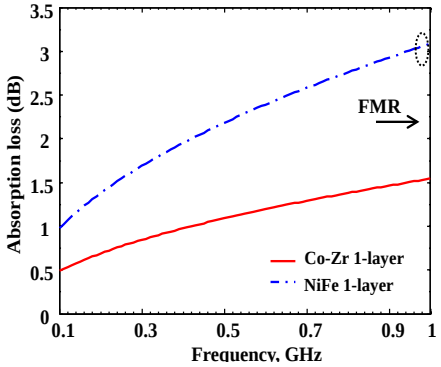

Figure 7. Comparison of absorption loss for NiFe and Co-Zr.

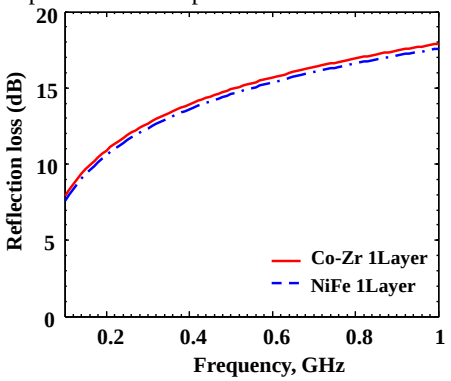

Figure 8. Comparison of reflection losses for NiFe and Co-Zr.

Since Co-Zr has a smaller 'σμ' product than NiFe, its absorption loss is lower, as seen in Figure 7. However, since both NiFe and Co-Zr have the same 'σ/μ' ratio, they have the same reflection loss. This is shown in Figure 8 (Note that the graph for NiFe has been slightly offset to distinguish the two plots). Here, the comparison is made upto 1GHz since NiFe exhibits FMR beyond ~1GHz and the comparison would not be valid beyond that.

For the multi-layered scenario, the simulations were performed with the equations for double-shielding derived in R.B. Schulz et al.[31] It was observed that for the multi-layer scenario, the loss due to reflection was much higher than the loss due to absorption. Figure 9 shows the total shield effectiveness (absorption + reflection losses+ multiple reflections due to thin shields) for single-layer and 10-layered stack of NiFe, for frequencies upto 1GHz (prior to FMR). Figure 10 shows the total shield effectiveness for single-layer and 10-layered stack of Co-Zr for frequencies upto 3GHz, prior to FMR. Comparing the results, the

following inferences can be made: a) NiFe with high absorption loss (A, defined in equation 8) has higher total shielding effectiveness than Co-Zr from 100MHz upto 1GHz because the effect of multiple reflections (B, defined in equation 9a) is suppressed; b) beyond 1GHz, NiFe can effect shielding through FMR absorption; c) Although less effective than NiFe under 1GHz, Co-Zr can provide shielding through reflection loss till upto 3 GHz, enabled by its higher FMR. It is to be noted that the total shielding effectiveness shown in Figure 9 and Figure 10 are ideal estimates and need to be modified for particular cases by taking into account the specific shield geometries and the presence of apertures.

Thus, through a combination of multi-layer structure and high-FMR materials, shielding can be made effective over a wider band of frequencies as desired, and the choice of material and the nanostructure would be dictated by the frequency band of the application.

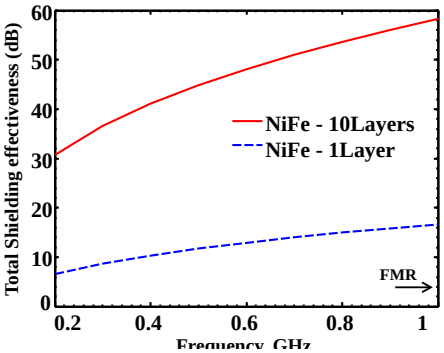

Figure 9. Shield effectiveness: single-layer and multi-layer NiFe. The FMR-related attenuation dominates above ~1 GHz for NiFe.

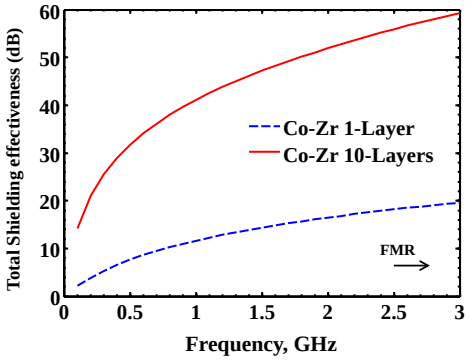

Figure 10. Shield effectiveness: single-layer and multi-layer CoZr. The FMR-related attenuation dominates above 3 GHz.

SUMMARY

Smart systems are driving new frontiers that require system scaling with advanced nanomaterials leading to nanostructured components. This paper describes the role of nanomagnetic materials for two such applications in system components – power inductors and EMI shield structures. The key material and geometry requirements for inductors and EMI isolation are described through analytical models. Co-Zr-O system is described as an exemplary nanomagnetic material system that provides key benefits in miniaturization and performance enhancement for these two applications because of its high M_s and H_k, and tunable resistivity depending on the oxygen content. With optimal oxygen content, the resistivity of Co-Zr-O is increased to suppress the eddy current losses for power inductors while Co-Zr alloys are more suitable for EMI shielding because of their high absorption and reflection losses from high permeability and high conductivity. Continuing advances in nanomagnetic laminates provide unique opportunities to further enhance these components in the future.

REFERENCES AND NOTES

1. F. Mazaleyrat, L. Varga. Ferromagnetic nanocomposites. *J. Magnetism and Magnetic Mat.* **2000**, 215, 253-59.
2. M. Wu, Y. Zhang, S. Hui, T. Xiao, S. Ge, W. Hines, J. Budnick, G. Taylor. Microwave magnetic properties of Co50/(SiO2) 50 nanoparticles. *Appl. Phys. Lett.* **2002**, 80, 4404-06.
3. M.A. Abshinova, A.V. Lopatin, N.E. Kazantseva, J. Vilčáková, P. Sáha. Correlation between the microstructure and the electromagnetic properties of carbonyl iron filled polymer composites. *Composites part A: Appl. Sci. Manufacturing* **2007**, 38, 2471-85.
4. R. Nowosielski. Soft magnetic polymer-metal composites consisting of nanostructural Fe-basic powders. *J. Achievements Mat. Manufacturing Engin.* **2007**, 24, 68-77.
5. J.N. Calata, G.-Q. Lu, K. Ngo. Soft Magnetic Alloy–Polymer Composite for High-Frequency Power Electronics Application. *J. Electronic Mat.* **2014**, 43, 126-31.
6. G. Herzer. Soft magnetic nanocrystalline materials. *Scripta Metallurgica et Materialia* **1995**, 33, 1741-56.
7. Y. Zhao, C. Ni, D. Kruczynski, X. Zhang, J.Q. Xiao. Exchange-coupled soft magnetic FeNi-SiO2 nanocomposite. *J. Physical Chem. B* **2004**, 108, 3691-93.
8. G. Herzer. Grain size dependence of coercivity and permeability in nanocrystalline ferromagnets. *IEEE Transactions on Magnetics* **1990**, 26, 1397-402.
9. R. Alben, J. Becker, M. Chi. Random anisotropy in amorphous ferromagnets. *J. Applied Physics* **1978**, 49, 1653-58.
10. H. Sato, O. Kitakami, T. Sakurai, Y. Shimada, Y. Otani, K. Fukamichi. Structure and magnetism of hcp-Co fine particles. *J. Applied Physics* **1997**, 81, 1858.
11. Y. Zhan, S. Wang, D. Xiao, J. Budnick, W. Hines. Nanocomposite Co/SiO2 soft magnetic materials. *IEEE Transactions on Magnetics* **2001**, 37, 2275-77.
12. Y. Hayakawa, A. Makino, H. Fujimori, A. Inoue. High resistive nanocrystalline Fe-MO (M= Hf, Zr, rare-earth metals) soft magnetic films for high-frequency applications. *J. Applied Physics* **1997**, 81, 3747-52.
13. S. Ohnuma, H. Fujimori, T. Masumoto, X. Xiong, D. Ping, K. Hono. FeCo–Zr–O nanogranular soft-magnetic thin films with a high magnetic flux density. *Appl. Phys. Lett.* **2003**, 82, 946-48.
14. S. Ge, D. Yao, M. Yamaguchi, X. Yang, H. Zuo, T. Ishii, D. Zhou, F. Li. Microstructure and magnetism of FeCo–SiO2 nano-granular films for high frequency application. *J. Phys. D: Applied Physics* **2007**, 40, 3660.
15. N.D. Ha, M.-H. Phan, C.O. Kim. Novel nanostructure and magnetic properties of Co–Fe–Hf–O films. *Nanotechnology* **2007**, 18, 155705.
16. P.M. Raj, H. Sharma, G.P. Reddy, N. Altunyurt, M. Swaminathan, R. Tummala, V. Nair. Cobalt–Polymer Nanocomposite Dielectrics for Miniaturized Antennas. *J Electronic Mat.* **2014**, 1-10.
17. P.M. Raj, H. Sharma, S. Samtani, D. Mishra, V. Nair, R. Tummala. Magnetic losses in metal nanoparticle-insulator nanocomposites. *J. Mat. Sci.: Materials in Electronics* **2013**, 24, 3448-55.
18. M. Darques, J. Spiegel, J. De la Torre Medina, I. Huynen, L. Piraux. Ferromagnetic nanowire-loaded membranes for microwave electronics. *J. Magnetism and Magnetic Mat.* **2009**, 321, 2055-65.
19. X. Kou, X. Fan, H. Zhu, R. Cao, J.Q. Xiao. Microwave Permeability and Tunable Ferromagnetic Resonance in Cobalt Nanowire Arrays. *IEEE Transactions on Magnetics* **2010**, 46, 1143-46.
20. Y. Shirakata, N. Hidaka, M. Ishitsuka, A. Teramoto, T. Ohmi. High permeability and low loss Ni–Fe composite material for high-frequency applications. *IEEE Transactions on Magnetics* **2008**, 44, 2100-06.
21. W. Yang, L. Qiao, J. Wei, Z. Zhang, T. Wang, F. Li. Microwave permeability of flake-shaped FeCuNbSiB particle composite with rotational orientation. *J. Appl. Phys.* **2010**, 107, 033913-13-5.

22. D. Guo, Z. Zhang, M. Lin, X. Fan, G. Chai, Y. Xu, D. Xue. Ni–Zn ferrite films with high resonance frequency in the gigahertz range deposited by magnetron sputtering at room temperature. *J. Phys. D: Appl. Phys.* **2009**, 42, 125006.
23. M. Sonehara, T. Sugiyama, T. Ishikawa, K. Inagaki, T. Sato, K. Yamasawa, Y. Miura. Relation between microwave complex permeability and ferromagnetic Fe-Si layer thickness in Mn-Ir/Fe-Si exchange-coupled film. *IEEE Transactions on Magnetics* **2006**, 42, 2984-86.
24. G. Chai, D. Xue, X. Fan, X. Li, D. Guo. Extending the Snoek's limit of single layer film in (Co96Zr4/Cu) n multilayers. *Appl. Phys. Lett.* **2008**, 93, 152516.
25. A.W. Lotfi, M.A. Wilkowski. Issues and advances in high-frequency magnetics for switching power supplies. *Proceedings of the IEEE* **2001**, 89, 833-45.
26. N.D. Ha, C.G. Kim, C.O. Kim, M.-H. Phan. Nanostructure and excellent magnetic properties of Co19. 35Fe53. 28Hf7. 92O19. 35 films. *Solid State Commun.* **2007**, 141, 502-05.
27. Y. Sun, C.R. Sullivan, W. Li, D. Kopp, F. Johnson, S.T. Taylor. Soft magnetic properties of obliquely deposited Co–Zr–O films. *IEEE Transactions on Magnetics* **2007**, 43, 4060-63.
28. H. Chang, J.J. Chen, V. Chen, S. Leou In *Microwave Conference Proceedings (APMC), 2012 Asia-Pacific* **2012**, p 920-22.
29. N. Karim, M. Jingkun, F. Jun In *Electromagnetic Compatibility (APEMC), 2010 Asia-Pacific Symposium on* **2010**, p 56-59.
30. H.W. Ott. Noise reduction techniques in electronic systems, 2nd ed. ed., New York: Wiley, **1988**.
31. R.B. Schulz, V.C. Plantz, D.R. Brush. Shielding theory and practice. *IEEE Transactions on Electromagnetic Compatibility* **1988**, 30, 187-201.
32. D.S. Gardner, G. Schrom, F. Paillet, B. Jamieson, T. Karnik, S. Borkar. Review of on-chip inductor structures with magnetic films. *IEEE Transactions on Magnetics* **2009**, 45, 4760-66.
33. H. Wu, S. Zhao, D.S. Gardner, H. Yu. Improved High Frequency Response and Quality Factor of On-Chip Ferromagnetic Thin Film Inductors by Laminating and Patterning Co-Zr-Ta-B Films. *IEEE Transactions on Magnetics* **2013**, 49, 4176-79.